The ISME Journal (2009) 3, 635–646

www.nature.com/ismej

ORIGINAL ARTICLE

Quantitative population dynamics of microbial communities in plankton-fed microbial fuel cells

Helen K White[1], Clare E Reimers[2], Erik E Cordes[1], Geoffrey F Dilly[1] and Peter R Girguis[1]
[1]*Biological Labs, Department of Organismic and Evolutionary Biology, Harvard University, Cambridge, MA, USA and* [2]*College of Oceanic and Atmospheric Sciences, Hatfield Marine Science Center, Oregon State University, Newport, OR, USA*

This study examines changes in diversity and abundance of bacteria recovered from the anodes of microbial fuel cells (MFCs) in relation to anode potential, power production and geochemistry. MFCs were batch-fed with plankton, and two systems were maintained at different potentials whereas one was at open circuit for 56.8 days. Bacterial phylogenetic diversity during peak power was assessed from 16S rDNA clone libraries. Throughout the experiment, microbial community structure was examined using terminal restriction fragment length polymorphism. Changes in cell density of key phylotypes, including representatives of *δ*-, *ε*-, *γ*-*proteobacteria* and *Flavobacterium-Cytophaga-Bacteroides*, were enumerated by quantitative PCR. Marked differences in phylogenetic diversity were observed during peak power versus the final time point, and changes in microbial community structure were strongly correlated to dissolved organic carbon and ammonium concentrations within the anode chambers. Community structure was notably different between the MFCs at different anode potentials during the onset of peak power. At the final time point, however, the anode-hosted communities in all MFCs were similar. These data demonstrate that differences in growth, succession and population dynamics of key phylotypes were due to anode potential, which may relate to their ability to exploit the anode as an electron acceptor. The geochemical milieu, however, governs overall community diversity and structure. These differences reflect the physiological capacity of specific phylotypes to catabolize plankton-derived organic matter and exploit the anode of an MFC for their metabolism directly or indirectly through syntrophy.
The ISME Journal (2009) **3,** 635–646; doi:10.1038/ismej.2009.12; published online 26 February 2009
Subject Category: microbial population and community ecology
Keywords: cell; fuel; plankton; power

Introduction

Microbial fuel cells (MFCs) are systems that harness energy as electrical current from microbial metabolism. Recent studies of MFCs have focused largely on the relationship between fuel composition, current efficiencies and power production (Liu *et al.*, 2005; Lovley, 2006; Rabaey *et al.*, 2007). To make MFCs commercially viable, studies have emphasized novel system designs (Liu and Logan, 2004), and synthesized microbial communities (Ren *et al.*, 2007). The majority of 'environmental' MFC studies, which do not use pure cultures, have examined the qualitative relationships between microbial diversity and power production (Rabaey *et al.*, 2004; Logan and Regan, 2006). Many of these studies have observed high bacterial diversity on the anodes, with high representation of *proteobacteria* and *Flavobacterium-Cytophaga-Bacteroides* (*FCB*; Holmes *et al.*, 2004; Reimers *et al.*, 2006, 2007). However, these studies examined bacterial diversity from 16S rDNA clone libraries, which reflect bacterial diversity at a single point in time, typically at the end of the incubations. More recent studies have shown qualitative changes in diversity do occur over time, and that power output from mixed microbial assemblages may be greater than pure cultures (Rabaey and Verstraete, 2005; Nevin *et al.*, 2008). Quantitative changes in microbial processes in relation to MFC performance, however, have not been examined. Without this quantitative data, it is impossible to determine the influence of geochemical and microbial processes, for example, organic matter degradation and population growth, on power production. It is also problematic to

Correspondence: PR Girguis, Biological Labs, Department of Organismic and Evolutionary Biology, Harvard University, 16 Divinity Avenue, Biolabs Room 3092, Cambridge, MA 2138, USA.
E-mail: pgirguis@oeb.harvard.edu
Received 8 October 2008; revised 26 January 2009; accepted 26 January 2009; published online 26 February 2009

determine the contribution of key phylotypes to power production in mixed communities. Because the majority of microbes in nature remain to be cultivated, quantitative molecular microbiological approaches must be used to examine the aforementioned relationships. Such approaches have been used successfully to determine population dynamics and cell-specific metabolic rates of uncultivated archaea in laboratory reactors (Girguis *et al.*, 2005).

The overarching goal of this study is to examine how biogeochemical and electrochemical processes interact to influence net changes in microbial ecology. In particular, we aimed to characterize the influence of anode potential and geochemical composition/concentration on the diversity, distribution and abundance of anode-hosted bacteria over time. To that end, we used three plankton-fed MFCs poised at different potentials to examine concomitant changes in power production, organic carbon and nitrogen composition and concentration, microbial diversity and distribution and quantitative changes in cell density of key phylotypes. Statistical analyses were used to determine which factors most significantly influence power production. These analyses enhance our understanding of microbial community succession toward exoelectrogenic competence, as well as the role of select phylotypes in different stages of power production.

Methods

Plankton-fed microbial fuel cell setup

In this study we used three plankton-fed MFCs, which derived both their organic matter and microbial inoculums from plankton and seawater (as in Reimers *et al.*, 2007). Each MFC was maintained in a lab at $15 \pm 3\,^{\circ}C$ and was composed of a stirred anaerobic anode chamber separated by a Nafion 117 membrane (DuPont Inc., Wilmington, DE, USA) from a cathode chamber containing circulating aerated seawater. Each chamber contained 19 graphite rods (152×9.5 mm; Graphite Engineering, Greenville, MI, USA) that were wired in parallel. The cathode and anode chambers were filled with 4.5 liters of 1 μm filtered seawater and 25 days later, ~36 g (wet weight) plankton (0.21–1 mm) collected from Oregon coastal waters was added to the anode chamber of each cell (we deliberately conducted these experiments in batch as it allowed us to more easily measure changes and ascertain relationships over time, a task not easily accomplished in continuous flow reactors). Potentiostats were then connected to control cell potentials, and electrical measurements were recorded every 15 min with a computerized data logger.

Two MFCs were held at whole-cell voltages of 0.3 and 0.6 V, whereas the third MFC was left at open circuit as a control. For convenience, we will hereafter refer to these as the 0.3, 0.6 V and the open-circuit or control MFC. The use of potentiostats resulted in anode potentials that did not vary much over time. Anode potentials equaled $+0.05 \pm 0.01$; -0.25 ± 0.04 and -0.45 ± 0.13 V vs Ag/AgCl (3 M KCl) for the 0.3, 0.6 V and open-circuit MFCs, respectively. The 0.3 and 0.6 V MFCs achieved different maximum currents of 2.5 and 5.2 mA, respectively. Peak power persisted from ~5 to 30 days after the plankton addition in the 0.3 V MFC, and from ~11 to 18 days in the 0.6 V MFC (Reimers *et al.*, 2007).

DNA extraction

Samples for microbial analyses were taken at 2.9, 5.9, 13.9, 27.9 and 56.8 days after plankton additions. Two anodes from each MFC were removed and scraped with a sterile razor blade. Scrapings were placed into 100 μl of 0.2 μm filter-sterilized 1:1 solution of ethanol and isoosmotic phosphate-buffered saline and frozen at $-80\,^{\circ}C$. Nucleic acids were extracted with the PowerSoil DNA extraction kit (MoBio Inc., San Diego, CA, USA) modified to normalize yields as in Girguis *et al.* (2005).

The contents of the plankton tow (discussed in Reimers *et al.*, 2007), which were used to inoculate and fuel the MFCs, were also sampled to assess the associated microbial community. Frozen plankton (4 g) were thawed, vortexed and centrifuged at 500 *g* to pellet the plankton and associated debris. The resulting supernatant was transferred to a clean tube, and DNA was extracted using a hexadecyltrimethylammonium bromide method (Doyle and Doyle, 1990), followed by ultracentrifugation through a cesium chloride/ethidium bromide gradient (as in Girguis *et al.*, 2005).

Clone libraries

Clone libraries were constructed for the 0.3 and 0.6 V MFC during the onset of peak power (5.9 and 13.9 days, respectively) as well as from the original plankton inoculum. Bacterial 16S rDNA genes were amplified by 25 cycles of PCR with bacterial-targeted forward primer (B27f, 59-AGAGTTTG ATCCTGGCTCAG-39) and a universal reverse primer (U1492r, 59-GGTTACCTTGTTACGACTT-39). Amplicons were cloned into a pCR4 TOPO vector and transformed into chemically competent *Escherichia coli* (TOPO TA cloning kit, Invitrogen Inc., Carlsbad, CA, USA). Transformants were screened on LB-kanamycin-X-GAL plates using blue-white selection. Plasmids were purified with the Montage miniprep kit (Millipore Inc., Billerica, MA, USA), and sequenced with BigDye chemistry (version 3.1) (Applied Biosystems Inc., Foster City, CA, USA) on an ABI 3730 capillary sequencer (Applied Biosystems Inc.). A total of 96 plasmids were sequenced in both directions for each library. SSU rDNA sequences were trimmed of vector using Sequencher 4.0 (Gene Codes Inc., Ann Arbor, MI, USA), then

compiled and aligned to full-length sequences with the Fastaligner alignment utility of the ARB program (www.arb-home.de). Alignments were verified by comparing each sequence's secondary structure with that of *E. coli*. Phylogenetic analysis of the SSU rDNA sequences was accomplished with MrBayes version 3.1.2 (www.mrbayes.csit.fsu.edu). The evolutionary model was set to the general time-reversible model, with rates equal to the inverse of γ. Two million generations were run, with sampling every 1000 generations, and burn-in was set to 20 000. SSU rDNA sequences described in this study were deposited in GenBank under accession numbers FJ664774 to FJ664821.

Terminal restriction fragment profiles

For terminal restriction fragment (T-RF) profiles, bacterial 16S rDNA genes were amplified with 5′ fluorescently labeled forward primer (B27f with a 6′-carboxyfluorescin) and a universal reverse primer (U1492r). Two independent 25 μl PCRs were performed for each sample and the products were combined and purified with a PureLink gel extraction kit (Invitrogen Inc.). Approximately 100 ng of purified amplicons was digested in separate 50 μl reactions with 10 U of *Hha*I, *Hin*fI and *Msp*I (New England Biolabs Inc., Ipswich, MA, USA) for 2 h at 37 °C. Triplicate T-RF profiles were obtained from the digested amplicons by suspending 1 μl aliquots in 8.75 μl formamide with 0.25 μl of GeneScan ROX 500 size standard (Applied Biosystems Inc.) and denaturing at 95 °C for 2 min. Separation of T-RFs was carried out on a 3730xl DNA sequencer (Applied Biosystems Inc.). T-RFs between 30 and 500 bp were analyzed using GeneMarker software version 1.6 (SoftGenetics LLC., State College, PA, USA). T-RF profiles were normalized for variable quantities of template by applying the variable percentage threshold as in Osborne *et al*. (2006), and aligned as described in Rees *et al*. (2004).

Statistical analyses of terminal restriction fragment profiles

Community structure was compared among MFCs with nonmetric multidimensional scaling (MDS) analysis of the T-RF profiles data using Primer 5 software (PRIMER-E, Lutton, UK, 2002). The data were transformed from percentages by taking the arcsine of the square root of each value. A matrix of pair-wise Bray–Curtis community similarity values was generated and used as the basis of the MDS analysis. This analysis arranges the T-RFs in two dimensions by an iterative procedure that optimizes the agreement between the relative distance between each pair of samples in the ordination space and the rank order of pair-wise community similarity. Spearman's rank correlation between the community similarity matrix and a matrix of Euclidean distance in measured electrical and chemical characteristics of the MFC was used to determine which factors best explained patterns in community similarity (as in Clarke and Warwick, 2001). The electrical and chemical characteristics included were current (square root transformed), ammonium ($\log x+1$ transformed), hydrogen sulfide ($\log x+1$ transformed), sulfate, dissolved inorganic carbon (DIC), dissolved organic carbon (DOC), particulate organic carbon (POC; $\log x+1$ transformed), particulate organic nitrogen (PON) and the particulate C/N ratio.

Design and development of quantitative PCR assays

Primers and TaqMan probes were designed and optimized for the dominant clones of *γ-proteobacteria*, *Geobacter* spp. (a *δ-proteobacteria*), *Arcobacter* spp. (an *ε-proteobacteria*) and *FCBs* (indicated by the letter P, Figure 1; Table 1). Primers were also designed for a more general *ε-proteobacteria* SYBR Green-based assay. Probes and primers were screened and optimized for TaqMan assays with Primer Express software (PE Biosystems Inc., Foster City, CA, USA) as in Girguis *et al*. (2005), and were checked for specificity by comparison to all available SSU rDNA sequences within ARB and BLAST (www.arbhome.de, NCBI). All quantitative PCR (qPCR) assays were performed on a Stratagene MX3000p sequence detector (Stratagene Inc., La Jolla, CA, USA) in 96-well optical grade plates. Each 30 μl PCR reaction contained the following reagents at final concentrations: 1 × TaqMan universal PCR master mix (containing AmpliTaq Gold DNA Polymerase; Applied Biosystems Inc.), varying concentrations of target-specific oligonucleotide primers (see Table 1) and 100 nM of each TaqMan probe. Additional ROX fluorescent dye and 1 U Platinum Taq (Invitrogen Inc.) were added to improve the signal to noise ratio. For the SYBR Green assay a final concentration of 1 × QuantiTect SYBR Green PCR Master Mix (Qiagen Inc., Valencia, CA, USA) and 500 nM of each primer was used. The amplification protocol was similar for all assays, except the annealing temperatures (Table 1). Amplification was carried out after 2 min at 50 °C, 10 min at 95 °C, 15 s at 95 °C and 1 min annealing at temperatures between 55 and 64 °C for 45 cycles (Table 1). Data analyses were carried out with the sequence detection system software MXPro (Stratagene Inc.). All reactions (standards, samples and blanks) were performed in triplicate and included a nontemplate control.

Quantitative PCR optimization

For optimization, each assay was performed with TaqMan probe concentrations of 100 nM, 150 mM and 200 mM, whereas PCR primer concentrations were systematically varied in all pair-wise combinations between 300 and 900 nM for both the forward and reverse primers. Optimum concentrations of TaqMan PCR primers are reported in Table 1.

Standardization for absolute quantification of target SSU rDNA genes

Standard curves for quantifying SSU rDNA gene copies were determined using plasmid DNA of

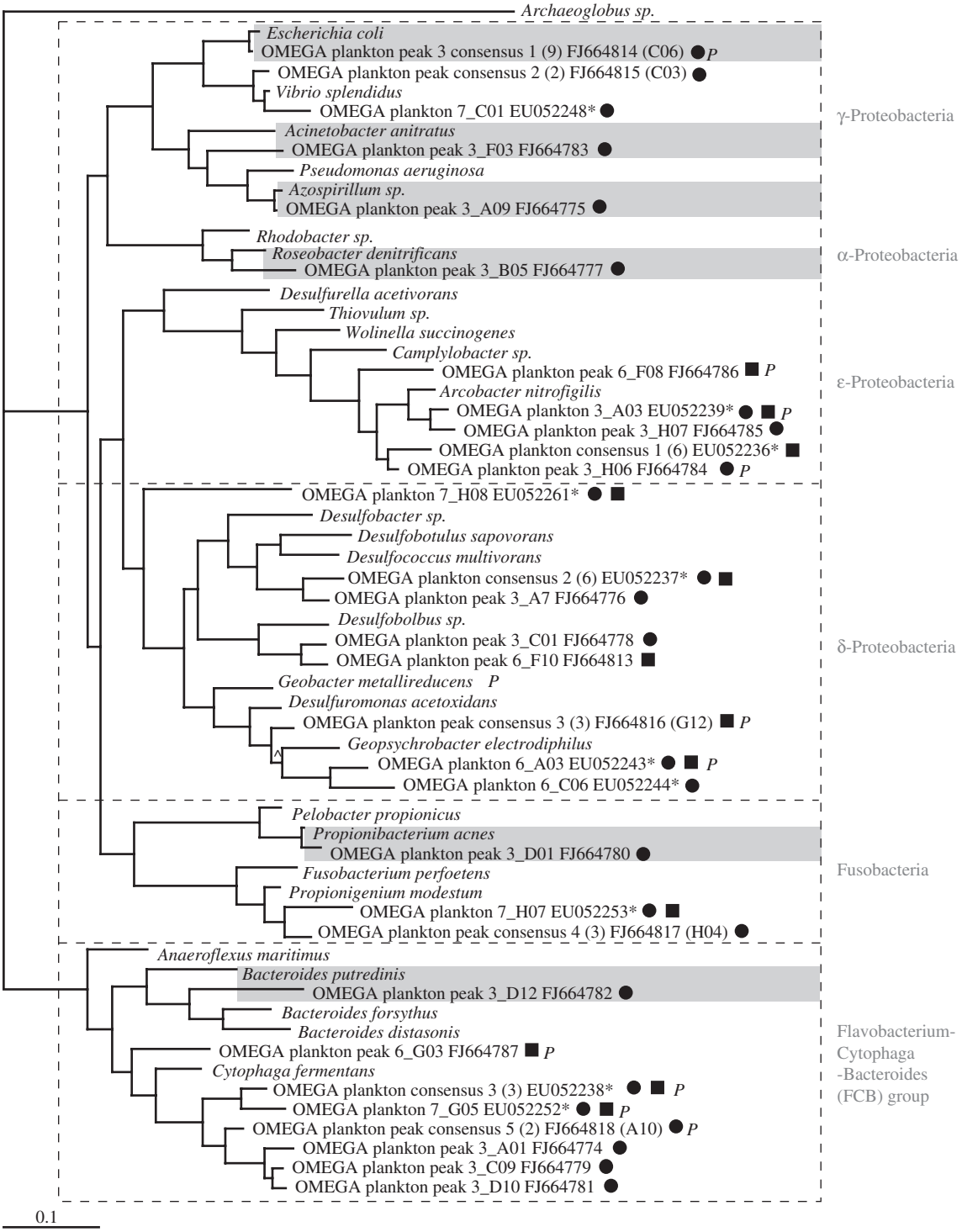

Figure 1 Phylogenetic tree constructed using Bayesian analysis, showing dominant phylotypes from anodes of 0.3 V (circles) and 0.6 V (squares) plankton-fed microbial fuel cells (MFCs) during peak power output. Trees constructed with other reconstruction algorithms (parsimony and maximum likelihood) resulted in the same overall topology. *Archaeoglobus* sp., an Archaeon, was used as the outgroup. Consensus sequences are indicated and the number of individual sequences contributing is shown in parentheses. Sequences that had been previously identified from end point samples (Reimers *et al.*, 2007) are noted with an asterisk and newly observed groups are highlighted with gray shading. Sequences used for primer and probe design are identified by '*P*'. Posterior probabilities were 1 except as indicated by '^' (0.5).

known concentration (10 ng μl^{-1}) from clones of interest (indicated by the letter P, Figure 1). Serial dilutions of nonlinearized plasmids spanning 6 orders of magnitude in copy number (1.67×10^0 to 1.67×10^6) were used to construct standard curves with r^2 values of 0.995–0.999 (Table 1). The number

Table 1 Real-time qPCR assay primer and probe concentrations and efficiencies

Assay name, primer and probe sequences	*Primer and probe conc. (nM)*	*Annealing temp. (°C)*	*Assay efficiency (%)*	r^2	*Min. detection (copies)*
Arcobacter spp. *(an ε-proteobacteria)*		60	81	0.995	43
98F: 5′-CGTAGAACGGGTATTAGCTTGCTAATA-3′	500				
280R: 5′-CCGTACAGTCYCATCCTAGAGCTATAA-3′	500				
Probe: 5′-CAAACGTTATCCCCTTCTCTAGGGCAGA-3′	100				
General ε-proteobacteria		60	87	0.999	40
93F: 5′-TGGCGSACGGGTGAGTAATRTATAG-3′	500				
409R: 5′-GGAGTTTACRCWCCGAAAWGYGTC-3′	500				
Geobacter spp. *(a δ-proteobacteria)*[a]		55	81	0.999	44
561F: 5′-GCGTGTAGGCGGTTTCTTAA-3′	900				
825R: 5′-TACCCGCRACACCTAGTTCT-3′	300				
Probe: 5′-CACTTCCTGGGTTGAGCCCAG-3′	100				
γ-Proteobacteria[b]		64	93	0.998	38
GAM F: 5′-CATGCCGCGTGTATGAAGAA-3′	300				
GAM R: 5′-CGGGTAACGTCAATGAGCAAA-3′	300				
Probe: 5′-TATTAAACTTTACTCCCTTCCTCCCCGCTGAA-3′	100				
Flavobacterium-Cytophaga-Bacteroides (FCB)		64	97	0.995	39
800F: 5′-CGAAGGCAGCTCACTAAACTAAYAT-3′	500				
1210R: 5′-CCTTGTARATTGCTCCGAAGAGAA-3′	500				
Probe: 5′-CTCAGTCACGCACRRTGTATYGTGC-3′	100				
Total bacteria[c]		60	87	0.998	41
331F: 5′-TCCTACGGGAGGCAGCAGT-3′	300				
797R: 5′-GGACTACCAGGGTATCTAATCCTGTT-3′	300				
Probe: 5′-CGTATTACCGCGGCTGCTGGCAC-3′	175				

[a]As in Stults *et al*. (2001).
[b]As in Huijsdens *et al*. (2002).
[c]As in Nadkarni *et al*. (2002).

of target rDNA gene copies in experimental samples was calculated using the standard curve and threshold cycle (C_t) of each PCR reaction using the equation: Copy number (Sample) = (C_t (Sample)–*y* Intercept (Standards))/(Slope (Standards)).

Cross-reactivity and inhibition

Cross-reactivity was examined for all qPCR assays using plasmid DNA containing SSU rDNA gene fragments from representatives of α-, δ-, ε- and γ-*proteobacteria*, *fusobacteria* and *FCB* recovered from the MFC (Table 1; Figure 1). Cross-reactivity was observed with the γ-*proteobacteria* assay and α-, ε- and δ-*proteobacteria* and *fusobacteria* plasmid DNA after 45 cycles. However, when quantified, non-target amplification was between 3 and 4 orders of magnitude less than target sequences for the γ-*proteobacteria* qPCR assay. With the *FCB* assay, cross-reactivity was observed with α-, γ-, ε- and δ-*proteobacteria* and *Fusobacteria*, but was also 3–4 orders of magnitude less than that of the targeted *FCB* plasmid DNA. No cross-reactivity was observed for the δ-*proteobacteria* or specific ε-*proteobacteria* assay. Cross-reactivity was observed with γ-*proteobacteria* with the general ε-*proteobacteria* assay, but was 3 orders of magnitude less than that of the targeted ε-*proteobacteria* plasmid DNA. Serial dilutions of DNA template (1- to 1000-fold) were performed to check for sample inhibition (none was observed).

Statistical analyses of phylotype abundance, electrochemical conditions and geochemical composition

Multiple regression analyses were run using Minitab version 15 (MiniTab Inc., State College, PA, USA) to identify environmental factors with the highest correlation to the cell densities of key phylotypes (as determined by qPCR). Cell densities of each phylotype were transformed by taking the arcsine of square root of each and were examined in separate models. Explanatory variables reported in Reimers *et al*. (2007) (current, ammonia, hydrogen sulfide, sulfate, DIC, DOC, POC, PON and the C/N ratio all transformed as before) were entered in the model at the start. After each iteration, the factor with the highest partial coefficient *P*-value is removed and the regression run again until only factors with *P*-values less than 0.05 are left. The best model is then selected based on the proportion of variance

explained (R^2 value) and the relative bias of the model (Mallow's Cp statistic).

Results

Microbial community composition at peak power

Significant differences were observed between clone libraries collected after the onset of peak power for 0.3 and 0.6 V MFC anodes (5.9 and 13.9 days, respectively). The 0.3 V MFC library had high representation of α- and *γ-proteobacteria* (allied with *Roseobacter denitrificans and Acinetobacter*, respectively) as well as phylotypes allied to *Propionibacterium acnes*. None of these phylotypes were observed in the 0.6 V MFC. Phylotypes allied with ε- and *δ-proteobacteria* as well as *FCB* were well represented in both MFCs (Figure 1).

Phylogenetic representation in the libraries constructed after the onset of peak power was notably different from that at the final time point (those recovered at peak power but not the final time point are highlighted in gray, Figure 1). Again, α- and *γ-proteobacteria*, as well as some members of the *Fusobacteria* and *FCB* group, were not observed at the final time point.

In contrast, the bacterial clone library generated from the initial plankton inoculum (Supplementary information) is dominated by α- and *γ-proteobacteria* (closely allied to phylotypes identified in 0.3 V MFC at peak power). However, the ε- and *δ-proteobacteria*, *Fusobacteria* and *FCB* phylotypes observed in the libraries generated during and after the MFC incubations were not represented in this library. Furthermore, phylotypes allied with *Planctomycetes* were also represented in the plankton inoculum library, but were not observed in any of the MFC incubation libraries. These clone libraries provide a coarse sense of microbial diversity among the different treatments, and illustrate the degree to which select phylotypes were enriched for during the MFC incubations.

Community structure

Microbial community structure was examined by the relative abundance of T-RFs within and between the MFCs over time (Figure 2). The average number of T-RFs per time point is 7 (s.d. = 2), ranging from 6 to 11, 3 to 10 and 4 to 12 for samples digested by restriction enzymes *Hha*I, *Hin*fI and *Msp*I, respectively. At 2.9 days, the communities of all three treatments are dominated (~40–80%) by T-RFs corresponding to an *FCB* (OMEGA plankton 7_A01 EU052246; with T-RF of 91 bp (*Hha*I), 178 bp (*Hin*fI) and 86 bp (*Msp*I)) and a *δ-proteobacteria* (OMEGA plankton 7_F05 EU052250; with T-RF of 92 bp (*Hha*I), 345 bp (*Hin*fI) and 162 bp (*Msp*I)). By 5.9 d, a shift in the 0.3 V MFC community is observed, and a new dominant phylotype appears, representing ~60% of the community with T-RF of 371 bp (*Hha*I), 329 bp (*Hin*fI) and 491 bp (*Msp*I) (Figure 2). This T-RF represents a *γ-proteobacteria* closely allied to *E. coli* (OMEGA plankton peak 3 consensus 1, Figure 1), as determined by *in silico* digestion of the clone libraries. The abundance of this phylotype is drastically reduced by 13.9 days (while elevated current was still being generated). The T-RF patterns suggest that the aforementioned *FCB* and *δ-proteobacteria* subsequently dominate the 0.3 V MFC. For the 0.6 V MFC, a significant change in community structure is not observed until 13.9 days (during peak power, Figure 2). In comparison, the open cell MFC exhibited less change in T-RF patterns, and is dominated by the aforementioned *FCBs* and *δ-proteobacteria* throughout the course of the incubation. By 56.8 days, the relative abundances of T-RFs in all three MFCs, including the open-circuit cell, were comparable. Most notably the *δ-proteobacteria* OMEGA plankton 7_F05 EU052250 decreased significantly in representation in all MFCs (Figure 2).

Statistical analyses of terminal restriction fragment profiles

The influence of four possible stressors (current, DOC concentration, ammonium concentration and sulfide concentration) on microbial community composition over time and among treatments was examined (Figure 3). Patterns in T-RF ordination reveal the degree to which the microbial communities are similar—communities from different time points and/or different MFCs that are similar cluster together. Notably, T-RF similarity was most highly correlated to ammonium (Figure 3c; $r = 0.465$, $P < 0.001$) and DOC (Figure 3b; $r = 0.435$, $P < 0.001$). Total current was also significant (Figure 3a; $r = 0.230$, $P = 0.018$), but explained less of the variance. Samples from 0.3 V MFC at 5.9 days and 0.6 V MFC at 13.9 days also display different community structures from the bulk of the samples. These communities correspond to the onset of a broad power peak in the 0.3 V cell and near the maximum of a sharper peak in the 0.6 V cell (Figure 3a; Reimers *et al.*, 2007). The communities at 56.8 days cluster together, indicating the similarity of the microbial communities at the final time point. These samples are also characterized by having the lowest concentrations of both DOC and ammonium compared to earlier time points (Figures 3b and c).

Phylotype abundance by q-PCR

Absolute changes in the cell density of the dominant ε- and *γ-proteobacteria*, *Geobacter* sp. and uncultured representatives of the *FCB* group during the course of the incubation are shown in Figure 4. Each phylotype's cell density is presented as the fraction of the total bacterial cell density. Some phylotypes have more than one copy of SSU rDNA genes (Fogel *et al.*, 1999). *Geobacter* sp. may have one

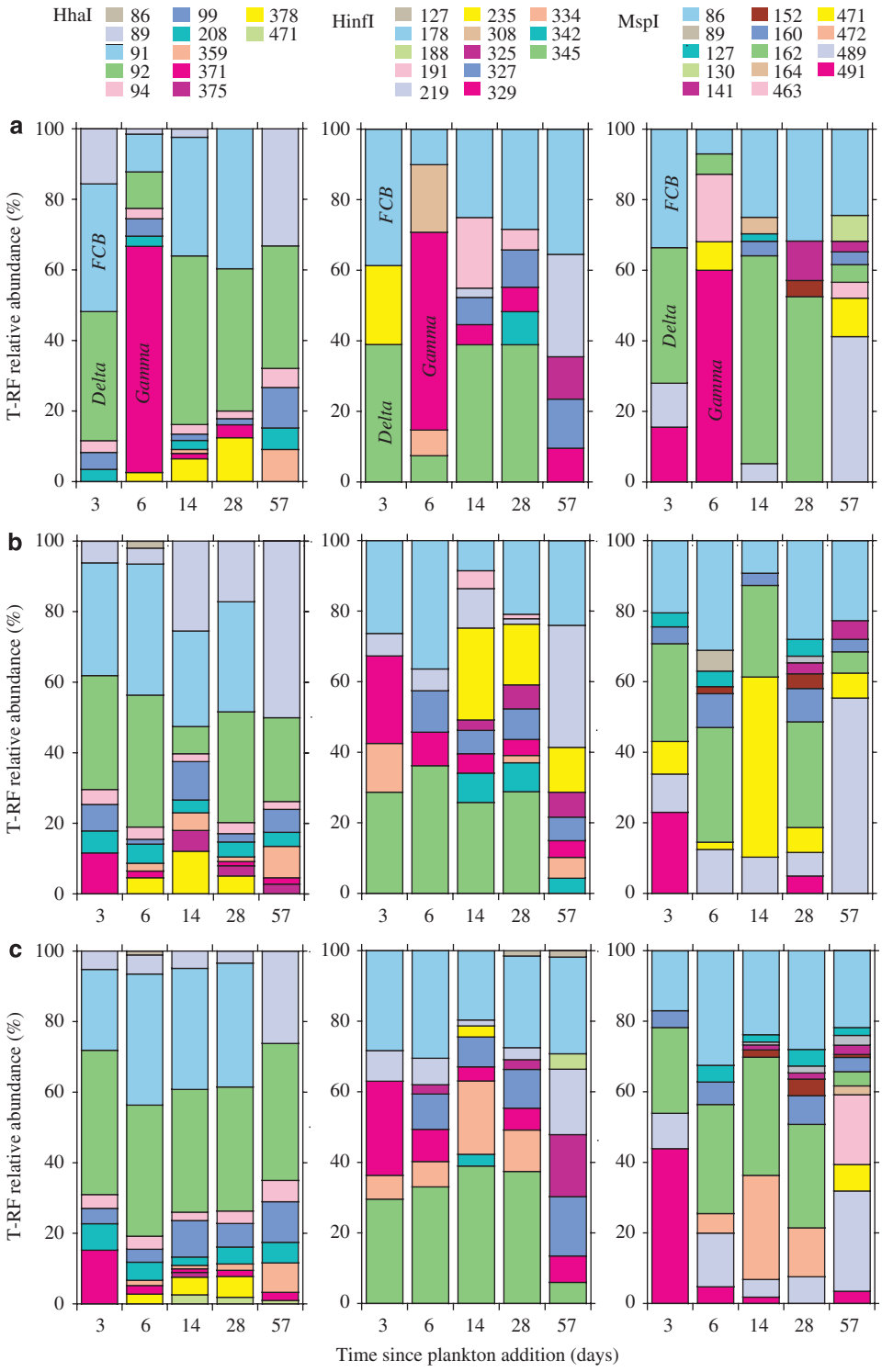

Figure 2 Relative abundances of bacterial terminal restriction fragments (T-RF) from (**a**) 0.3 V, (**b**) 0.6 V and (**c**) open-circuit control microbial fuel cells (MFCs), after digestion with *Hha*I, *Hin*fI and *Msp*I. Numbers next to colored squares represent T-RF size in base pairs. Dominant phylotypes identified by *in silico* digestion of clone libraries are identified as *Flavobacterium-Cytophaga-Bacteroides* (*FCB*) (OMEGA plankton 7_A01 EU052246; with T-RF of 91 bp (*Hha*I), 178 bp (*Hin*fI) and 86 bp (*Msp*I)), an uncultured *δ-proteobacteria* (OMEGA plankton 7_F05 EU052250; with T-RF of 92 bp (*Hha*I), 345 bp (*Hin*fI) and 162 bp (*Msp*I)) and uncultured *γ-proteobacteria* (OMEGA plankton peak 3 consensus 1; with T-RF of 371 bp (*Hha*I), 329 bp (*Hin*fI) and 491 bp (*Msp*I)).

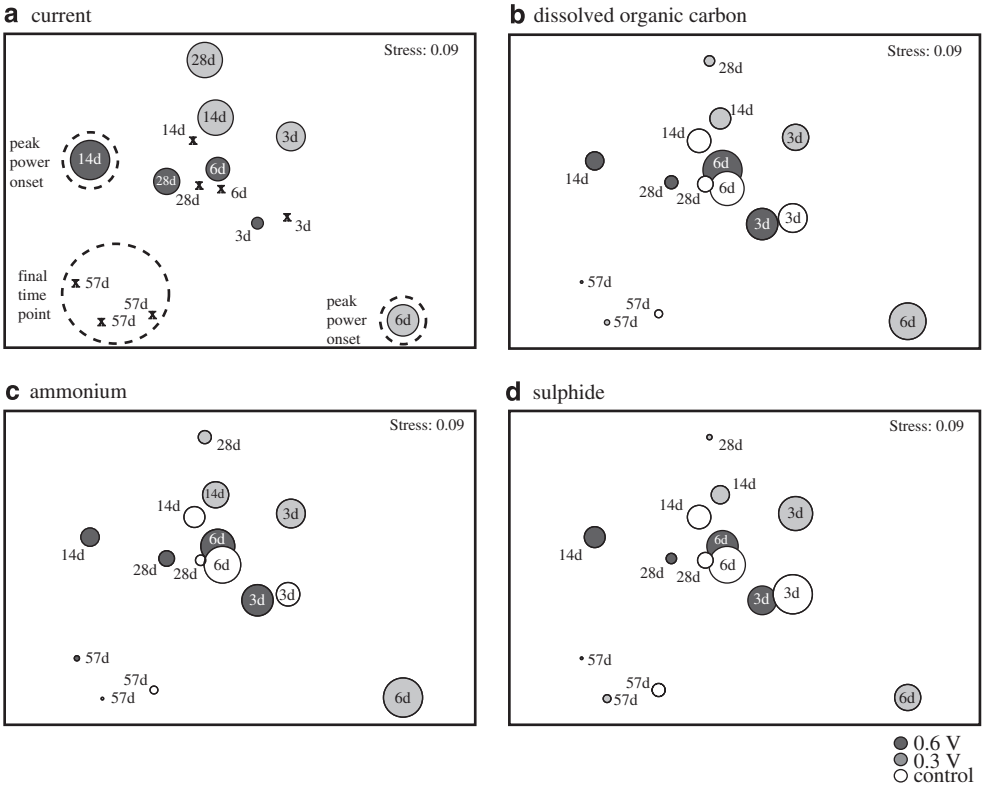

Figure 3 Multidimensional scaling (MDS) plot of terminal restriction fragment (T-RF) profile similarity. Area of circles represents magnitude of (**a**) current, (**b**) dissolved organic carbon, (**c**) ammonium and (**d**) sulfide. The letter 'x' represents zero values for these parameters. Numbers represent sampling points in days (rounded to nearest whole number). Dashed circles in panel (**a**) highlight T-RF profiles at peak power and the final time point in all treatments.

copy (Holmes *et al.*, 2004); *Campylobacter* sp., closely related to the uncultured *ε-proteobacteria* in this study, has between three and seven copies (Wesley *et al.*, 1995); *E. coli* may have up to seven copies (Fogel *et al.*, 1999), whereas some *FCB* have one copy (Fogel *et al.*, 1999). Any bias produced by a phylotype with multiple SSU rDNA gene copies would be less than an order of magnitude, and thus less than any differences in phylotype abundance discussed here.

The 0.3 V MFC experienced a significant increase in *γ-proteobacteria* abundance at the onset of peak power (5.9 days), which constituted 18% of the bacterial population (Figure 4a). By 13.9 days, the *γ-proteobacteria* are displaced by *Geobacter*, which have increased to 19% of the total bacterial population. By 27.9 days, *Geobacter* and *ε-proteobacterial* cell densities are comparable at 4% of the total bacterial population, and continue to decline over time. *γ-Proteobacterial* cell densities further decrease over this same interval (Figure 4a).

In the 0.6 V MFC, *Geobacter* spp. dominate at four of five time points, including peak power, and comprise between 33% and 51% of the bacterial population (Figure 4b). *ε-Proteobacterial* cell density increases in the 0.6 V MFC at the onset of peak power, representing 15% of the total bacterial population. To determine if *ε-proteobacterial* growth is dominated by the most common phylotype represented in the clone library, namely *Arcobacter nitrofigilis* (Figure 1), we developed a highly specific qPCR assay targeting these phylotypes. This assay showed an increase of *A. nitrofigilis* at peak power that represented 2% of the total bacterial population. *γ-Proteobacteria* were below our limits of detection throughout this incubation (Figure 4b).

FCB phylotypes were present in all anode samples, and temporal changes in their abundance were similar between treatments, with a peak at 5.9 days in the 0.3 V (54%; Figure 4a) and open-circuit cells (47%; Figure 4c) and at 13.9 days in the 0.6 V MFC (31%; Figure 4b).

Multiple regression analyses of the qPCR data suggest that POC ($P = 0.037$) and ammonium ($P = 0.041$) concentrations were most significantly related to the variability in the abundance of *Geobacter* spp. ($r^2 = 0.730$). DOC may have an additional effect, but was marginally significant ($P = 0.057$). None of the potential explanatory factors examined was related to the relative abundance of the *γ-* and *ε-proteobacteria*. For the *FCBs*, seven of the nine factors appear to contribute to the variability ($r^2 = 0.690$), with sulfide concentrations being the most significant ($P = 0.039$; negatively correlated).

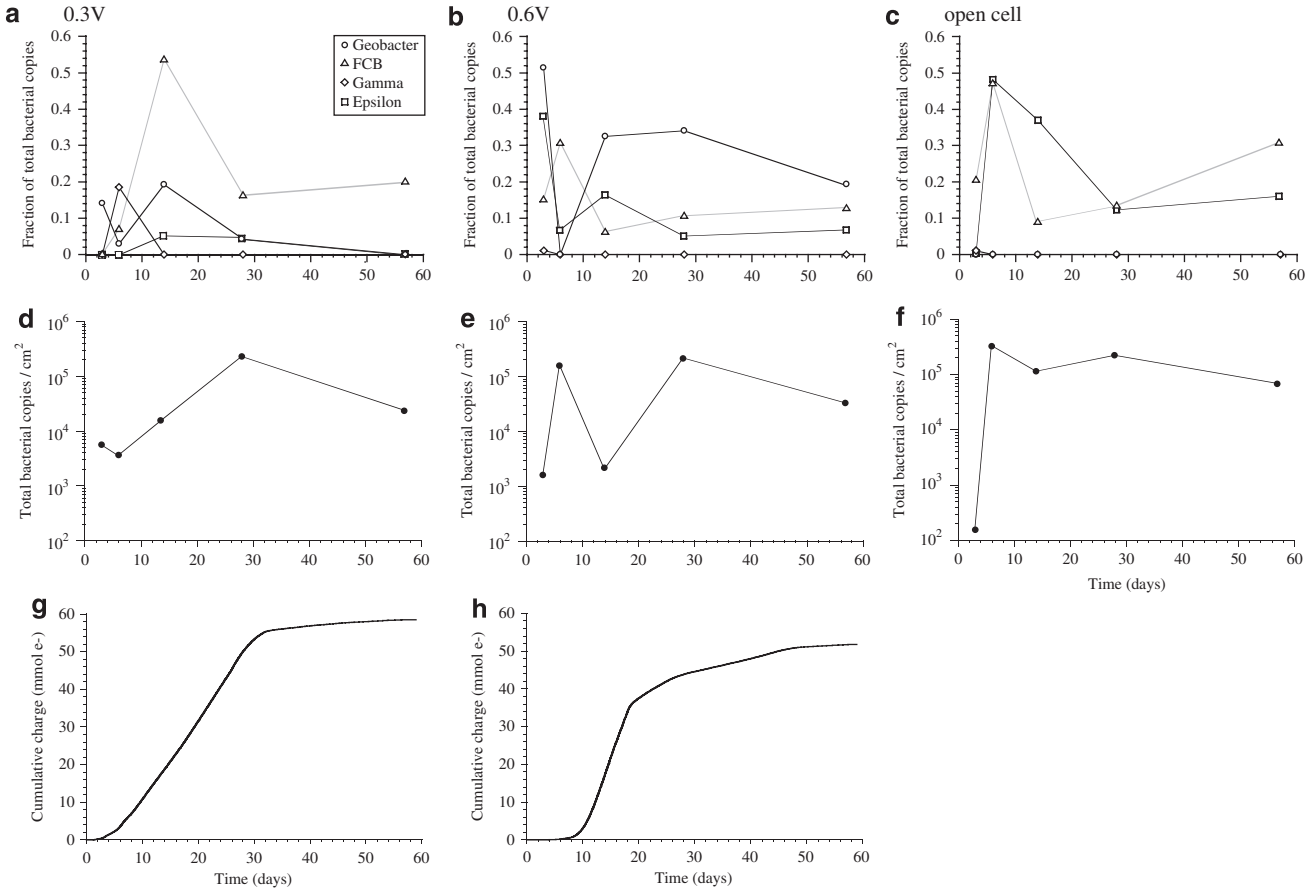

Figure 4 Cell density of *δ*-, *γ*- and *ε-proteobacteria*, as well as *Flavobacterium-Cytophaga-Bacteroides* (*FCB*) phylotypes in (**a**) 0.3 V, (**b**) 0.6 V and (**c**) open-circuit microbial fuel cells (MFCs) as determined by qPCR. Cell densities are depicted as the percent fraction of total bacterial copies determined by qPCR for (**d**) 0.3 V, (**e**) 0.6 V and (**f**) open-circuit in each MFC, and are normalized to anode surface area. $N = 3$ for all points, and standard error bars are smaller than symbols shown. Cumulative charge (mmol per electron) is shown for (**g**) 0.3 V and (**h**) 0.6 V MFCs, respectively.

Discussion

The data presented here provide the first quantitative demonstration of changes in cell densities of key phylotypes during power production in environmental MFCs, and illustrate the complex relationships between electrochemical state, geochemistry, power production and microbial ecology. Despite the high degree of similarity in the geochemical milieu between treatments (see Reimers *et al.*, 2007), there are quantifiable differences in the cell density and population dynamics of *γ*-, *δ*- and *ε-proteobacteria* within anode biofilms. It has previously been suggested that only certain phylotypes within an anode biofilm can maximize their energy gain for a given anode potential, or that only some species have a mechanism to adjust the potential of their reductases to be slightly negative of the electrode (Finkelstein *et al.*, 2006). These data provide empirical support for this idea, and suggest that the observed patterns are due to the differences in anode potential between MFCs. The succession observed in the 0.3 V MFC (from *γ-proteobacteria* to *Geobacter*, and the eventual dominance of *FCB* phylotypes over 5.9–27.9 days, Figure 4a) suggests that *γ-proteobacteria* competed effectively for resources, and possibly contributed to power production (discussed below) within the anode biofilm during the onset of peak power. However, both *Geobacter* and *FCB* succeeded them and later dominate during ongoing power production.

The succession and population dynamics observed in the 0.6 V MFC differ in that *Geobacter* dominates from the onset of peak power through the duration of the incubation (whereas *γ-proteobacteria* remain undetectable, less than 50 cells; Figure 4b). A substantial decrease in bacterial cell density is observed at the onset of peak power (13.9 days; Figure 4e) in the 0.6 V MFC that is not observed in the other MFCs. Excluding the possibility of substantial differences between individual rods (drawn from these well-mixed anode chambers), this suggests that power production affects bacterial cell density. We posit that the anode is initially colonized by a wider variety of phylotypes during the first few days of incubation, and that at the onset of power production certain phylotypes, including exoelectrogens such as *Geobacter* and some

γ-proteobacteria, or those which are syntrophically coupled to exoelectrogens, increase in abundance (Figure 4b). Higher-resolution temporal studies would further test this hypothesis.

The role of *ε-proteobacteria*, as well as *FCBs*, in power production remains unconstrained. *Geobacter* and other *δ-proteobacteria* are known exoelectrogens (Lovley, 2006), and *γ-proteobacteria*, including *E. coli*, have been shown to be capable of extracellular electron transfer via exogenous electron shuttles (Roller *et al.*, 1984; McKinlay and Zeikus, 2004). As such, these *γ-proteobacteria* may be physiologically capable of exploiting the anode as an electron acceptor, and the data shown here provide evidence for this notion because there is increasing power production in the 0.3 V MFC whereas *γ-proteobacterial* cell densities increase and *Geobacter* cell densities decrease (though notably the majority of power produced in the 0.3 V MFC occurs after the *γ-proteobacterial* cell density is diminished; Figure 4a). The observed increase in *ε-proteobacteria* cell density during peak power production in both the 0.3 and 0.6 V MFCs suggests they too may contribute to power production. *ε-Proteobacteria* are associated with particulate organic matter and are capable of low molecular weight DOC and sulfide oxidation (DeLong *et al.*, 1993; Covert and Moran, 2001; Wirsen *et al.*, 2002). They are ubiquitous in aquatic ecosystems and are important in cycling carbon and sulfur (Campbell *et al.*, 2006). They have also been found in other MFCs (Aelterman *et al.*, 2008). However, the abundance of *ε-proteobacteria* in the anode biofilms in all MFCs (including the open-circuit MFC) may also indicate a response to the availability of sulfide or its electrochemical oxidation product (elemental sulfur), and their capacity to transfer electrons to an MFC anode remains to be tested.

The presence of *FCBs* on MFC anodes suggests a potentially syntrophic relationship that supports power production. During these experiments, *FCBs* were always present on MFC anodes during closed and open-circuit conditions. *FCBs* are known degraders of complex organic compounds (Covert and Moran, 2001; Kirchman, 2001 and references therein) and have previously been identified on the anodes of benthic MFCs (Reimers *et al.*, 2006). Their capacity to degrade complex organics into simpler organic acids may explain the observed covariance of *FCB* and *Geobacter* cell density and distribution over time in the 0.3 V MFC (Figure 4a). This would also serve to explain how these communities sustain power production after the first 30 days of incubation, when complex, less-reactive, organic carbon is the prevalent carbon source (Reimers *et al.*, 2007). Future experiments should further examine this relationship.

The quantitative changes in cell density of key phylotypes show that anode-hosted communities exhibit successional patterns that reflect each phylotype's capacity to compete for resources, including the anode as a terminal electron acceptor, during the course of the incubation. Such ecological interactions likely influence the total charge transfer (Figures 4d–f). In the 0.3 V MFC, the cumulative charge transferred to the anode does not correlate or bear similarity to the growth of any one phylotype. However, at 0.6 V, cumulative charge is similar in curvature to that of *Geobacter* growth (though marginally significant; $P = 0.067$, Spearman's rank coefficient). These data suggest that at the anode potential and geochemical conditions in the 0.3 V MFC, several phylotypes including *Geobacter* may be competing for resources, and differentially contributing to power production, whereas in the 0.6 V MFC, *Geobacter* appears to be most competitive. It is also possible that other members of the anode biofilm that were not quantified may have contributed to power production, or deterred from power production through antagonistic interaction.

The T-RF patterns provide a qualitative means of examining changes in community structure over time and it is apparent that anode biofilm community structure is predominantly influenced by the geochemical milieu (Figure 3). However, at peak power in both the 0.3 and 0.6 V MFCs, the community structures (as represented by the T-RF patterns) bear little resemblance to other time points or each other, further supporting the idea that the influence of the anode potential on the anode biofilm supersedes that of the geochemical milieu. Nevertheless, these data show that geochemical factors can differentially and significantly affect anode-hosted phylotypes, influencing their growth regardless of their contribution to power production during the course of the experiment. More accurately, it is the metabolic activity of the bacterioplankton, which are primarily responsible for the observed changes in geochemical composition that influence anode-hosted communities. This factor has not been well addressed in previous studies of aqueous- or sediment-hosted MFCs, and these data clearly suggest that future studies should consider and examine the relationship between bacterioplankton (and sediment-hosted microbes) and the anode-hosted biofilm.

In sum, power production in MFCs fueled by complex organic carbon (such as plankton, sludge or wastewater) is governed by a complex series of ecological, geochemical and electrochemical interactions. The temporal resolution and quantitative approaches used in this study allow us to observe trends between the anodic microbial community, fuel and power production for the first time, and illustrate the degree to which anode potential, geochemistry and time influence microbial ecology. It is evident that the anode potential dictates, to a first order, the growth, population dynamics and ecological succession of known and putative exoelectrogenic phylotypes within the anode-hosted biofilm. These ecological dynamics subsequently influence current density and power production.

The geochemical milieu, in turn, influences the microbial community to a second order, inducing changes in anode-hosted community diversity and structure throughout the duration of the experiment, regardless of a phylotype's contribution to power production. Overall, these data underscore the need for further quantitative investigations of microbial ecology in laboratory and field-deployed MFCs. Future studies should aim to investigate the physiological and ecological relationships between anode-hosted phylotypes. Consideration should also be given to the planktonic microbial community within the anode chamber, whose activity is largely responsible for temporal changes in the geochemical milieu. We suggest that future investigations endeavor to use quantitative molecular approaches (such as qPCR or fluorescent *in situ* hybridization) to advance our understanding of how quantitative changes in microbiological factors influence system performance.

Acknowledgements

We thank Yvan Alleau, Kate A Howell, Sonam Sharma, Hilmar A Stecher III, Lisa Steinberg and Benjamin Wolfe for technical assistance. Support for this research came from grants provided by DARPA and the Office of Naval Research and a Harvard University Microbial Science Initiative (MSI) postdoctoral fellowship to H White.

References

Aelterman P, Rabaey K, De Schamphelaire L, Clauwaert P, Boon N, Verstraete W. (2008). Microbial fuel cells as an engineered ecosystem. In: Wall JD, Harwood CS, Demain AL (eds). *Bioenergy*. ASM: Washington, DC.

Campbell BJ, Engel AS, Porter ML, Takai K. (2006). The versatile ε-proteobacteria: key players in sulphidic habitats. *Nat Rev Microbiol* **4**: 458–468.

Clarke KR, Warwick RM. (2001). *Change in Marine Communities: An Approach to Statistical Analysis and Interpretation*, 2nd edn. Primer-E Ltd.: Plymouth, United Kingdom.

Covert JS, Moran MA. (2001). Molecular characterization of estuarine bacterial communities that use high- and low-molecular weight fractions of dissolved organic carbon. *Aquat Microbiol Ecol* **25**: 127–139.

DeLong EF, Franks DG, Alldredge AL. (1993). Phylogenetic diversity of aggregate-attached vs free-living marine bacterial assemblages. *Limnol Oceanogr* **38**: 924–934.

Doyle JJ, Doyle JL. (1990). Isolation of plant DNA from fresh tissue. *Focus* **12**: 13–15.

Finkelstein DA, Tender LM, Zeikus JG. (2006). Effect of electrode potential on electrode-reducing microbiota. *Environ Sci Technol* **40**: 6990–6995.

Fogel GB, Collins CR, Li J, Brunk CF. (1999). Prokaryotic genome size and SSU rDNA copy number: estimation of microbial relative abundance from a mixed population. *Microb Ecol* **38**: 93–113.

Girguis PR, Cozen A, DeLong EF. (2005). Growth rates of methane-oxidizing archaeal-bacterial consortia in deep-sea marine sediments: insights into the physiology of microbially-mediated anaerobic methane oxidation. *Appl Environ Microbiol* **71**: 3725–3733.

Holmes DE, Bond DR, O'Neil RA, Reimers CE, Tender LR, Lovley DR. (2004). Microbial communities associated with electrodes harvesting electricity from a variety of aquatic sediments. *Microb Ecol* **48**: 178–190.

Huijsdens XW, Linskens RK, Mak M, Meuwissen SGM, Vandenbroucke-Grauls CMJE, Savelkoul PHM. (2002). Quantification of bacteria adherent to gastrointestinal mucosa by real-time PCR. *J Clin Microbiol* **40**: 4423–4427.

Kirchman DL. (2001). The ecology of *Cytophaga-Flavobacteria* in aquatic environments. *FEMS Microbiol Ecol* **39**: 91–100.

Liu H, Cheng S, Logan BE. (2005). Production of electricity from acetate or butyrate using a single-chamber microbial fuel cell. *Environ Sci Technol* **39**: 658–662.

Liu H, Logan BE. (2004). Electricity generation using an air-cathode single chamber microbial fuel cell in the presence and absence of a proton exchange membrane. *Environ Sci Technol* **38**: 4040–4046.

Logan BE, Regan JM. (2006). Electricity-producing bacterial communities in microbial fuel cells. *Trends Microbiol* **14**: 512–518.

Lovley DR. (2006). Microbial energizers: fuel cells that keep on going. *Microbe* **1**: 323–329.

McKinlay JB, Zeikus JG. (2004). Extracellular iron reduction is mediated in part by neutral red and hydrogenase in *Escherichia coli*. *Appl Environ Microbiol* **70**: 3467–3474.

Nadkarni MA, Martin FE, Jacques NA, Hunter N. (2002). Determination of bacterial load by real-time PCR using a broad-range (universal) probe and primers set. *Microbiology* **148**: 257–266.

Nevin KP, Richter H, Covalla SF, Johnson JP, Woodard TL, Orloff AL *et al.* (2008). Power output and columbic efficiencies from biofilms of *Geobacter sulfurreducens* comparable to mixed community microbial fuel cells. *Environ Microbiol* **10**: 2505–2514.

Osborne CA, Rees GN, Bernstein Y, Janssen PH. (2006). New threshold and confidence estimates for terminal restriction fragment length polymorphism analysis of complex bacterial communities. *Appl Environ Microbiol* **72**: 1270–1278.

Rabaey K, Boon N, Verhaege M, Verstraete W. (2004). Biofuel cells select for microbial consortia that self-mediate electron transfer. *Appl Environ Microbiol* **70**: 5373–5382.

Rabaey K, Rodriguez J, Blackall LL, Keller J, Gross P, Batstone D *et al.* (2007). Microbial ecology meets electrochemistry: electricity-driven and driving communities. *ISME J* **1**: 9–18.

Rabaey K, Verstraete W. (2005). Microbial fuel cells: novel biotechnology for energy generation. *Trends Biotechnol* **23**: 291–298.

Rees GN, Baldwin DS, Watson GO, Perryman S, Nielsen DL. (2004). Ordination and significance testing of microbial community composition derived from terminal fragment length polymorphisms: application of multivariate statistics. *Antonie Leeuwenhoek* **86**: 339–347.

Reimers CE, Girguis PR, Stecher III HA, Tender LM, Ryckelynck N, Whaling P. (2006). Microbial fuel cell energy from an ocean cold seep. *Geobiology* **4**: 123–136.

Reimers CE, Stecher III HA, Westall JC, Alleau Y, Howell KA, Soule L *et al.* (2007). Substrate degradation kinetics, microbial diversity and current efficiency of microbial fuel cells supplied with marine plankton. *Appl Environ Microbiol* **73**: 7029–7040.

Ren Z, Ward TE, Regan JM. (2007). Electricity production from cellulose in a microbial fuel cell using a defined binary culture. *Environ Sci Technol* **41**: 4781–4786.

Roller SD, Bennetto HP, Delaney GM, Mason JR, Stirling JL, Thurston CF. (1984). Electron-transfer coupling in microbial fuel cells: 1. Comparison of redox-mediator reduction rates and respiratory rates of bacteria. *J Chem Technol Biotechnol* **34**: 3–12.

Stults JR, Snoeyenbos-West O, Methe B, Lovley DR, Chandler DP. (2001). Application of the 5′ fluorogenic exonuclease assay (TaqMan) for quantitative ribosomal DNA and rRNA analysis in sediments. *Appl Environ Microbiol* **67**: 2781–2789.

Wesley IV, Schroeder-Tucker L, Baetz AL, Dewhirst FE, Paster BJ. (1995). Arcobacter-specific and *Arcobacter butzleri*-specific 16S rRNA-based DNA probes. *J Clin Microbiol* **33**: 1691–1698.

Wirsen CO, Sievert SM, Cavanaugh CM, Molyneaux SJ, Ahmad A, Taylor LT *et al.* (2002). Characterization of an autotrophic sulphide-oxidizing marine *Arcobacter* sp. that produces filamentous sulphur. *Appl Environ Microbiol* **68**: 316–325.

Supplementary Information accompanies the paper on The ISME Journal website (http://www.nature.com/ismej)